Journal of Catalysis 278 (2011) 143–152

Contents lists available at ScienceDirect

Journal of Catalysis

journal homepage: www.elsevier.com/locate/jcat

Heterogeneous catalysis with supported platinum colloids: A systematic study of the interplay between support and functional ligands

X. Wang [a], P. Sonström [a], D. Arndt [a], J. Stöver [b], V. Zielasek [a,c], H. Borchert [d], K. Thiel [c], K. Al-Shamery [b], M. Bäumer [a,*]

[a] Institute of Applied and Physical Chemistry, University of Bremen, Leobener Str. NW 2, 28359 Bremen, Germany
[b] Institute of Pure and Applied Chemistry, University of Oldenburg, Carl-von-Ossietzky-Str. 9-11, 26129 Oldenburg, Germany
[c] Fraunhofer Institute for Manufacturing Technology and Applied Materials Research (IFAM), Wiener Str. 12, 28359 Bremen, Germany
[d] EHF Laboratory, Department of Physics, University of Oldenburg, Carl-von-Ossietzky-Str. 9-11, 26129 Oldenburg, Germany

ARTICLE INFO

Article history:
Received 28 August 2010
Revised 22 November 2010
Accepted 24 November 2010
Available online 6 January 2011

Keywords:
Pt nanoparticles
Organic ligand shell
Support effect
Octadiene hydrogenation
CO oxidation

ABSTRACT

Whereas colloidal metal nanoparticles have attracted considerable interest in homogeneous catalysis, the effect of organic ligands has been less systematically investigated in heterogeneous gas-phase catalysis. This paper aims at elucidating this aspect for nanoparticles capped with dodecylamine (DDA), which have been deposited on three different support materials with varying acid/base properties, namely γ-Al_2O_3, SiO_2 and MgO. For this purpose, a synthetic approach was applied that is based on the preparation of *ligand-free* Pt nanoparticles in ethylene glycol. By functionalizing these particles *subsequently* with ligands, it is possible to obtain ligand-free and ligand-capped particles with the same metal core (e.g. identical size and shape), thus allowing to investigate the influence of the ligands without changing any other parameter. After deposition on the different supports, the Pt nanoparticles were characterized by STEM, AAS and DRIFTS. The catalytic properties of these catalysts were investigated under two different reaction regimes: first, octadiene hydrogenation served as a test reaction to probe the influence of the ligands on larger molecules under reducing conditions at low temperatures ($T < 100$ °C) where the ligand shell is intact. The results show that ligands can strongly modify metal–support interactions and exert a protecting effect with respect to support induced oxidation of Pt surface atoms that occurs during particle deposition. In particular, in the case of the Brønsted acidic SiO_2 support, where surface oxidation of Pt is most pronounced, the ligand-capped sample is significantly more active for octadiene hydrogenation than the ligand-free counterpart. Second, the samples were tested with respect to CO oxidation at high temperatures ($T \sim 200$ °C) where processes like decomposition/desorption and spillover of ligands on the support become important. Depending on the acid/base and adsorption properties of the different supports, the spillover of DDA turns out to be the main reason for diminishing the ligand coverage of the nanoparticles under these conditions. Whereas spillover is most pronounced on Lewis acidic γ-Al_2O_3, a specific interaction between the basic MgO and DDA, namely its catalytic transformation into a nitrile, leads to enhanced spillover when compared to the Brønsted acidic SiO_2. These observed ligand effects are not limited to catalysts synthesized with the ethylene glycol method but are also observed in the case of the particles prepared by a classical colloidal approach.

1. Introduction

Methods traditionally used for the preparation of heterogeneous catalysts, such as impregnation or precipitation, generally allow only limited structural control. Therefore, the application of colloidal chemistry offering extensive possibilities to modify the size and shape of particles and to control the composition has attracted considerable interest both in homogeneous and in heterogeneous catalysis. Catalytically interesting systems, which have meanwhile been prepared with well-defined morphologies and narrow size distributions, are Au [1,2], Pt [2–4], Pd [5,6], Co [1,7,8], Fe [7,9], Co–Pt [10,11], Co–Pd [11], and Fe–Pt [12] nanoparticles to name just a few. Different strategies, such as simple colloidal deposition [13], binding via surface-anchored ligands [14], embedding in the network of a polymer [15] or porous inorganic oxide matrices [16], have been proposed and proved to be effective for the immobilization of such metal or alloy nanoparticles on supports.

Very often, colloidal nanoparticles are surrounded by a shell of organic ligands or polymers, which were added during the

* Corresponding author.
E-mail address: mbaeumer@uni-bremen.de (M. Bäumer).

0021-9517/$ - see front matter © 2010 Elsevier Inc. All rights reserved.
doi:10.1016/j.jcat.2010.11.020

synthesis to stabilize the particles during the growth process. Whereas in homogeneous catalysis such ligand shells are present under typical reaction conditions, in heterogeneous gas-phase catalysis, the fate of the organic ligand shells and their influence on the catalytic properties are usually unclear. Based on the assumption that catalytic activity is diminished if the surface of the metal nanoparticles is partly covered by organic ligands, the ligand shells were often removed in previous studies either by extraction or pyrolysis prior to catalytic applications [17–20]. Yet, the subsequent removal might lead to undesirable structural changes, such as changes in shape or even sintering [21].

In addition, the removal of ligands might be short-sighted from another viewpoint as for (quasi-)homogeneous catalysis carried out in the liquid phase a number of studies reported very beneficial effects of ligands, directing e.g. selectivity or even resulting in enantioselectivity [22–24]. In heterogeneous gas-phase catalysis, although interesting perspectives to prevent sintering or to modify the interaction with the support – possibly steering metal–support interactions – exist also here, the effect of ligands was less intensively investigated [25–27].

In a previous study, we have shown that small molecules, such as CO and O_2, can easily penetrate a ligand shell of dodecylamine, reversibly adsorb on supported colloidal Pt nanoparticles and react on the surface to CO_2 [28]. For larger molecules, like benzene or pyridine, the accessibility of the metal core in the presence of ligands has been recently reported [29,30]. Apart from the reactants, it is also important to consider the reaction conditions, when trying to assess the influence of ligands. At the higher temperatures typical of CO oxidation, ligands can partly desorb or decompose or, as reported in another study from our laboratory, spillover on the support [31].

Since organic ligands are generally present when colloidally synthesized nanoparticles are used in catalysis, a systematic study of the catalytic properties of ligand-capped nanoparticles is desirable, which takes into account possible structural changes under reaction conditions, the influence of the ligand shell on metal–support interactions *and* the fate of organic ligand shells. Aiming at a quantitative and not just qualitative comparison, appropriate reference systems without ligands are necessary, which, however, are often missing. A traditionally prepared catalyst will in most cases be different with respect to structure (e.g. particle size) and composition.

In this work, we address and overcome this problem by adopting a strategy for the preparation of *identical* unprotected and ligand-capped Pt nanoparticles, which is based on a synthetic approach using ethylene glycol (EG) as a solvent. It was previously shown that Pt, Ru, Rh [32], Os, Pt–Rh [33], and Pt–Ru [34] nanoparticles exhibiting sufficient stability in alkaline EG without protective agents can be obtained in this way. These particles can then be covered with organic ligands in a *subsequent* step. Aiming at a detailed analysis to which degree ligands affect the catalytic performance, their coverage can be changed by offering different ligand concentrations during the functionalization. To the best of our knowledge, this is the first study systematically investigating the influence of ligands on heterogeneous gas-phase catalysis by using *identical* colloidally synthesized nanoparticles *with* and *without* ligands.

After depositing the Pt nanoparticles on three different supports (SiO_2, MgO and γ-Al_2O_3) with varying acid/base properties, we carried out two different types of catalytic reactions: the hydrogenation of an olefin – here 1,7-octadiene was used because it was assumed that it cannot penetrate the ligand shell easily – and the oxidation of CO using uncovered and ligand-capped Pt particles. While in the first case low temperatures (<100 °C) and reductive conditions were applied, CO oxidation allowed studying the behavior under oxidative conditions and higher temperatures. It turned out that, depending on the acid/base and adsorption properties of the different supports, spillover processes can take place, reducing the coverage of ligands on the metal particles significantly. Still, during preparation, i.e. deposition of the particles, the ligands are able to decouple the particles from the support efficiently so that e.g. negative effects due to surface oxidation of the particles, particularly affecting the hydrogenation reaction, can be avoided.

2. Experimental section

2.1. Chemicals

Dihydrogen hexachloroplatinate (IV) hexahydrate ($H_2PtCl_6{\cdot}6H_2O$, Pt wt.% = 40%) was purchased from ChemPur. Platinum tetrachloride ($PtCl_4$) was purchased from Acros Organics. Sodium hydroxide (NaOH, 99%) was supplied by Riedel-de Haën. Dodecylamine (DDA), didodecyldimethyl ammonium bromide (DDAB), and tetrabutyl ammonium borohydride (TBAB) were obtained from Aldrich. 1,7-octadiene was purchased from Merck. All organic solvents used in this work were of analytical grade.

Aluminum oxide (γ-Al_2O_3, Alfa Aesar), magnesium oxide (MgO, Acros Organics), and silicon oxide (SiO_2, Johnson Matthey) were used as received.

2.2. Preparation of "unprotected" Pt nanoparticles

The method used in this work for the preparation of "unprotected" Pt nanoparticles is similar to one reported previously [32]. In a typical experiment, an EG solution of $H_2PtCl_6{\cdot}6H_2O$ (50 mL, 41 mM) was added into an EG solution of NaOH (50 mL, 400 mM) under stirring to obtain a transparent yellow platinum hydroxide or oxide colloidal solution, which was then heated at 160 °C for 3 h, with an inert gas flow passing through the reaction system to remove water and organic byproducts. A transparent dark-brown homogeneous colloidal solution of Pt metal nanoparticles (20.5 mM, 4.0 g Pt/L) was obtained without any precipitation. The as-prepared Pt nanoparticles in EG are very stable; no aggregation was observed under ambient atmosphere for several months.

2.3. Preparation of ligand-capped Pt nanoparticles

For the preparation of DDA-capped Pt nanoparticles, a phase-transfer method was adopted by using the "unprotected" Pt nanoparticles as precursors. As illustrated in Scheme 1, a diluted EG solution (10 mL) of "unprotected" Pt nanoparticles (10.3 mM) was added dropwise into a toluene solution (10 mL) of DDA. The concentration of DDA in toluene was varied between 20.5 and 103 mM to obtain different degrees of coverage of the Pt surface. The obtained mixture of two phases was stirred at room temperature for 3 h and then rested for 1 h to form distinct two phases, i.e. an upper toluene phase of ligand-capped Pt nanoparticles and a bottom EG phase. The EG phase was removed and the toluene phase was washed with water three times, which was then concentrated to ~0.5 mL under flowing N_2. To this concentrated solution, 10 mL of ethanol was added to precipitate the products, which were subsequently isolated by centrifugation and washed with ethanol three times to remove free ligands. The washed precipitates of ligand-capped Pt nanoparticles were finally dissolved in chloroform to produce a stable colloidal solution.

2.4. Preparation of ligand-capped and ligand-free Pt catalysts

For the deposition of ligand-free and ligand-capped Pt catalysts, three support materials (γ-Al_2O_3, SiO_2 and MgO) differing in their

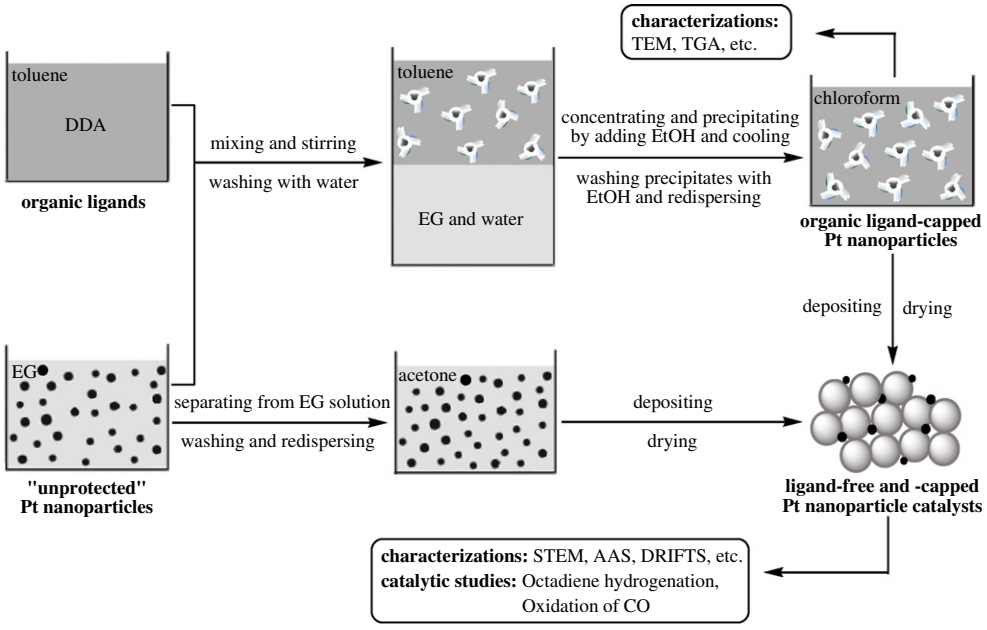

Scheme 1. Illustrative diagram of the methods for the preparation of ligand-free and ligand-capped Pt catalysts.

surface acidity were used. In order to characterize the acid/base properties of the used supports, DRIFTS measurements were carried out with pyridine [35–37] as a probe molecule. The absorption bands indicated Lewis acidity for γ-Al_2O_3, Brønsted acidity for SiO_2 and no surface acidity at all for MgO (data not shown). Colloidal solutions of DDA-capped Pt nanoparticles in chloroform (as prepared according to Section 2.3) were added to the required amounts of γ-Al_2O_3, MgO and SiO_2, respectively. The mixture was stirred manually until the solvent evaporated completely. Additionally, for comparison, γ-Al_2O_3 presaturated with DDA by ultrasonification of the powdered material in a 80 mM solution of DDA in toluene was also used as a support. The Pt loading of all samples investigated in this study was identical, as determined by atomic absorption spectroscopy (AAS). The obtained catalysts were dried in vacuum overnight before they were used for characterizations and reactions.

For the preparation of ligand-free Pt catalysts (Scheme 1), the "unprotected" Pt nanoparticles (as prepared according to Section 2.2) were first precipitated by adding an aqueous solution of HCl (15 mL, 1 M) to lower the pH value of the Pt colloidal solution in EG (5 mL, 20.5 mM). After centrifugation, the obtained precipitates of "unprotected" Pt nanoparticles were washed with the HCl aqueous solution three times, then redispersed in acetone and finally deposited on the corresponding catalyst supports according to the steps described above.

2.5. Preparation of DDA-capped Pt nanoparticles according to the method of Jana and Peng

To obtain DDA-capped Pt nanoparticles by a classical colloidal approach first described by Jana and Peng [2], $PtCl_4$ (8.5 mg) was dissolved in a toluene solution (2.5 mL) of the DDA ligand (186 mg). Under vigorous stirring at room temperature, didodecyldimethyl ammonium bromide (DDAB) and tetrabutyl ammonium borohydride (TBAB) were added as solubilizer and reducing agent, respectively (25 mg TBAB in 1 mL of a 0.1 M solution of DDAB in toluene). The reaction was completed after ~30 min, and the nanoparticles were precipitated with methanol, redissolved in hexane, and precipitated once again with a mixture of methanol and acetone (1:4). The product was then dissolved in hexane prior to deposition on the support materials. Results reported throughout the article for DDA-capped Pt nanoparticles refer in general to the ethylene glycol method (preparation according to Section 2.3), only where explicitly stated the colloidal approach described here was used.

2.6. Characterization of the nanoparticles and the catalysts

Transmission electron microscopy (TEM) measurements were carried out by using a Tecnai F20 S-TWIN microscope (FEI) operated at 200 kV to characterize the structural properties of "unprotected" and ligand-capped Pt nanoparticles. Samples for TEM measurements were prepared by placing a drop of the diluted EG solution of "unprotected" Pt nanoparticles on a carbon-coated copper grid or by dipping the grid in the chloroform solution of ligand-capped Pt nanoparticles. Thermogravimetric analysis (TGA) was employed by using a TGA/SDTA-851e instrument from Mettler-Toledo to check the thermal stability and the weight fraction of organic ligands on Pt nanoparticle surfaces. In this way, it was possible to determine the suitable temperature region for catalytic reactions and to estimate the surface coverage of Pt nanoparticles. The TGA samples were obtained by evaporating the chloroform solution of DDA-capped Pt nanoparticles followed by drying the samples in vacuum overnight. 10 mg of the sample was deposited in a pierced Al pan. Data were collected in the temperature range of 25–600 °C with a heating rate of 10 °C/min and a nitrogen flow of 70 mL/min. Besides, scanning transmission electron microscopy (STEM) and atomic absorption spectroscopy (AAS) measurements were conducted on catalyst powders to evaluate the dispersion of metal particles on the supports and to analyze the metal loading of catalysts, respectively. For AAS measurements, an AAS 5FL Flame from Zeiss was used and operated with an acetylene/nitrous oxide flame after dissolving the samples in aqua regia, boiling for 1 min and leaving them overnight.

2.7. Octadiene hydrogenation

The hydrogenation of 1,7-octadiene was investigated in a suitable laboratory reactor (fixed-bed type reactor with a heating system) for the ligand-free and ligand-capped Pt catalysts under

Table 1
Particle size distribution of ligand-free and DDA-capped Pt samples.

Sample	Support	Average size of Pt particles[a]	Mean deviation[a]	Fig. 1
Pt	no[b]	2.04 nm	±0.35 nm	a
DDA–Pt		2.00 nm	±0.31 nm	b
Pt	γ-Al_2O_3 (before)[c]	2.18 nm	±0.23 nm	c
DDA–Pt		1.95 nm	±0.22 nm	d
Pt	γ-Al_2O_3 (after)[d]	2.21 nm	±0.29 nm	e
DDA–Pt		2.04 nm	±0.28 nm	f

[a] Determined by measuring more than 200 nanoparticles found in arbitrarily chosen areas in the TEM images.
[b] TEM grids were directly prepared from the colloidal solution.
[c] Fresh samples, TEM grids were prepared directly after deposition onto the support.
[d] After use of the catalysts for one cycle of CO oxidation ($T_{max} \sim 200$ °C).

continuous-flow conditions. A gas flow containing 7 vol.% H_2 (balance: He, total flow: 50 mL/min) was directed through a saturator kept at 7 °C (corresponding to a saturated gas phase with 0.9 vol.% octadiene) containing the liquid diene. The components in the product stream were analyzed with a Fisons GC 8000 series equipped with a TRIO 1000 quadrupol mass spectrometer. A CP-Porabond-Q column (25 m, 0.25 mm, 3 μm) was used to separate octadiene, isomers of octene (mainly 1-octene), and octane isothermally at 200 °C with He as a carrier gas. Precautions were taken to avoid mass-transport limitations and electrostatic charging: the powder catalysts were pressed and sieved into 0.31–0.45 mm grains, from which 10 mg were then mixed with quartz (800 mg, diameter 0.4–0.8 mm, Roth, calcinated at 1000 °C for 6 h) and placed between quartz wool into the reactor.

2.8. CO oxidation

For CO oxidation experiments, the same laboratory reactor as described in Section 2.7 was used. The samples were again pressed in grains and mixed with quartz before measuring under continuous-flow conditions. The components in the product stream were analyzed with a photometric detector for CO/CO_2 (URAS 3G, Hartmann & Braun).

Additionally, in situ IR spectroscopy for CO oxidation was performed in diffuse-reflectance geometry (DRIFTS) with a Biorad FTIR spectrometer (FTS-60 A). Catalyst samples were pressed into pellets and investigated in a reaction cell equipped with a heating unit and a controlled gas supply system for in situ studies. All spectra were recorded with a resolution of 2 cm^{-1} under continuous gas flow with Ar as the carrier gas.

Turnover frequencies (TOFs) were calculated by assuming spherical particle shape and accessibility of all Pt surface atoms. Because all Pt particles are in contact with the support and a part of their surface is not available for CO oxidation, the calculated TOF values represent lower limits.

3. Results

3.1. Structural characterization

In Fig. 1a, a TEM image of "unprotected" Pt nanoparticles is displayed, revealing that they have a quasi-spherical shape and an average diameter of 2.04 nm ± 0.35 nm. According to HRTEM, the particles are single-crystalline (see the inset in Fig. 1a). Fig. 1b, on the other hand, shows a TEM image of the DDA-capped Pt nanoparticles. The average particle size and size distribution of these nanoparticles are in agreement with the "unprotected" Pt nanoparticles (Table 1), indicating that the structural properties of Pt nanoparticles are not changed during the ligand functionalization process. It is also worth noting that the ligand-capped nanoparticles are well-separated from each other even though the TEM sample was prepared with a solution of high Pt concentration. Accordingly, the ligand shells can efficiently prevent particles from agglomeration.

The next preparation step comprised the deposition of the ligand-free and ligand-capped particles on different catalyst supports. The corresponding STEM images are shown exemplarily for γ-Al_2O_3 in Fig. 1c and d. (Similar STEM images were obtained for the other supports used in this study.) EDX analyses confirmed that the small bright spots in the images are Pt nanoparticles, which are well-dispersed on the supports. The data thus prove that the colloidal deposition method adopted in this work is well-suited for depositing Pt nanoparticles on various catalyst supports without causing obvious aggregation of the metal nanoparticles.

3.2. Octadiene hydrogenation

The hydrogenation of 1,7-octadiene was chosen as a test reaction to investigate the influence of the amine ligand shell on catalytic activity and selectivity on supported Pt nanoparticles at low temperatures ($T < 100$ °C) under *reductive* conditions, e.g. conditions under which the ligand shell is stable. As shown by kinetic studies for this non-conjugated diene, sequential hydrogenation of the double bonds should dominate, but parallel hydrogenation may play a minor role as well [38].

Fig. 2 compares the activities and selectivities of Al_2O_3-supported Pt nanoparticles with and without DDA as a ligand using a fourfold stoichiometric excess of hydrogen to exclude a lack of H_2 being responsible for partial hydrogenation products. First, all three samples are highly active and reach full conversion at temperatures far below 100 °C, showing that even large molecules, such as octadiene, can easily penetrate the ligand shell and are converted at the metallic core. In detail, the ligand-free sample was found to have the highest activity (full conversion of 1,7-octadiene at 45 °C), while the activities of the DDA-capped samples (with identical metal loading) were slightly lower. Additionally, with an increasing amount of ligands, the conversion curves were slightly shifted to higher temperatures. Assuming an activation energy for the hydrogenation reaction of about 40 kJ/mol [39], which is not significantly changed by the presence of the ligand shell, the temperature shift can be straightforwardly explained by the blocking of Pt surface sites. Based on an Arrhenius approach, it can be estimated that a reduction of the number of active sites by 50% (DDA–Pt 2/1) and 65% (DDA–Pt 10/1) would account for the temperature increase. This is in agreement with a study by Fu et al. [40], reporting a ligand coverage of ~50% for DDA-capped Pt prepared by the same method with a DDA/Pt ratio close to 2/1.

Turning to selectivity, Fig. 3 reveals that for a given conversion no significant changes in the product selectivity are observed, when comparing the uncovered particles and the ligand-capped particles. Additional experiments with smaller H_2/octadiene ratios also led to a shift of the conversion curves to higher temperatures

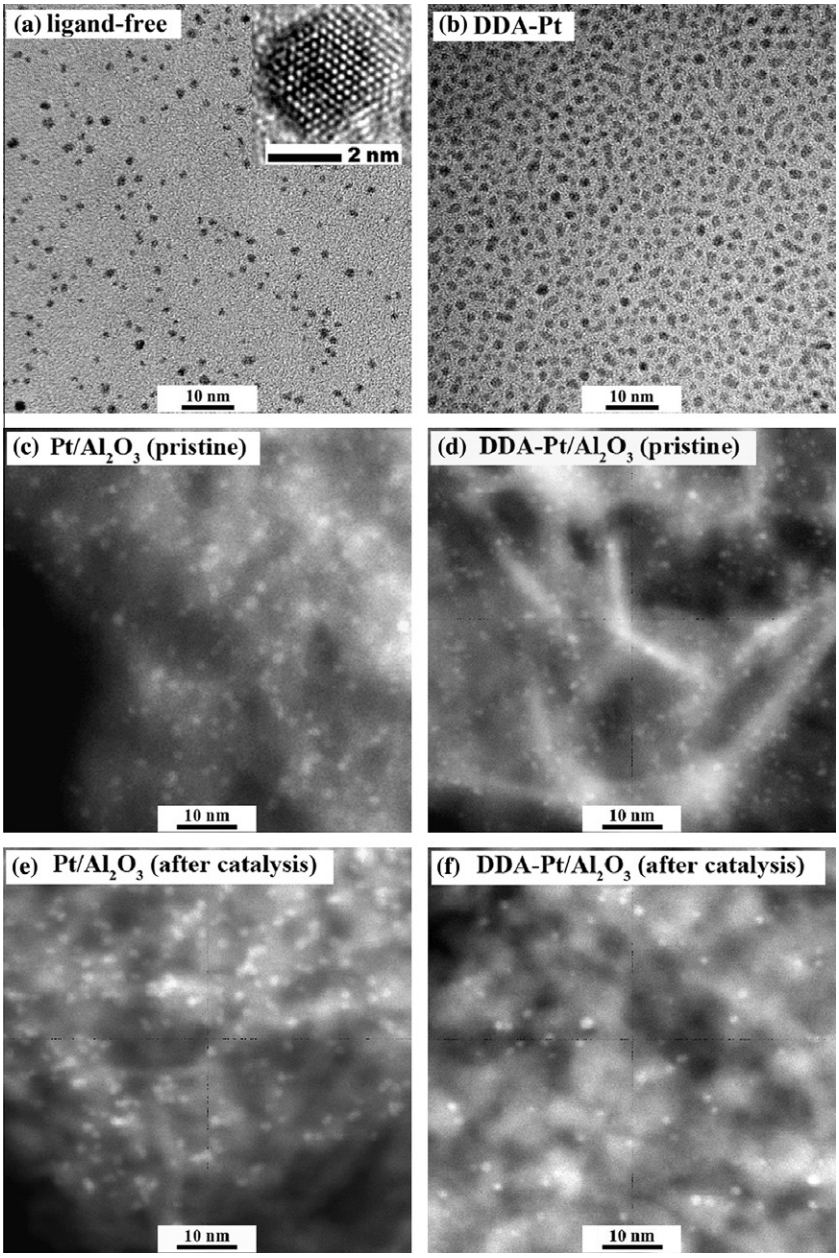

Fig. 1. TEM images of (a) "unprotected" Pt nanoparticles (inset: HRTEM showing the crystallinity of a single nanoparticle) and (b) DDA-capped Pt nanoparticles prepared with the ethylene glycol method. STEM images of (c) "unprotected", (d) DDA-capped Pt nanoparticles directly after deposition on γ-Al_2O_3, (e) "unprotected" and (f) DDA-capped, alumina-supported Pt samples after use for CO oxidation.

but yielded also comparable selectivities for a given conversion. (Please note that larger amounts of octene were only observed when hydrogen was used under-stoichiometrically, e.g. offering only enough H_2 to react with *one* of the two double bonds.) Interestingly, the almost linear relationship between selectivity and conversion that can be inferred from Fig. 3 is only expected for $k_2/k_1 \approx 2$, with k_2 being the rate constant for the hydrogenation of octene to octane and k_1 the rate constant for the hydrogenation of octadiene to octene (assuming pseudo first order rate laws). A ratio of about 2 for k_2/k_1 was indeed reported for the competitive hydrogenation of 1,7-octadiene and alkenes (e.g. hexene, heptene) [41]. Since the same trends were also observed for the nanoparticles supported on MgO instead of Al_2O_3 (data not shown), the data suggest that, in the case of these two supports, the reaction of octadiene hydrogenation is not influenced by the ligand shells. In particular, the kinetic behavior is identical and differences can be solely attributed to a lower number of active sites.

The catalytic activities and selectivities of a ligand-free and DDA-capped Pt sample supported on SiO_2 shown in Fig. 4 however reveal differences. Whereas still an almost linear relationship between selectivity and conversion is observed (data not shown), the ligand-free particles are now significantly less active than the ligand-capped ones, which in turn exhibit a similar activity than the ligand-capped particles supported on the other supports. We will address the reasons for the difference observed for the ligand-free particles in detail in Section 4.1.

3.3. CO oxidation

CO oxidation was conducted to investigate the effect of the amine ligand shell on the catalytic activities of the Pt nanoparticles at *higher* temperatures ($T \sim 200$ °C) and under *oxidative* conditions. The results are displayed in Fig. 5. Apparently, the ligand-free Pt nanoparticles supported on γ-Al_2O_3, MgO, and SiO_2 show basically

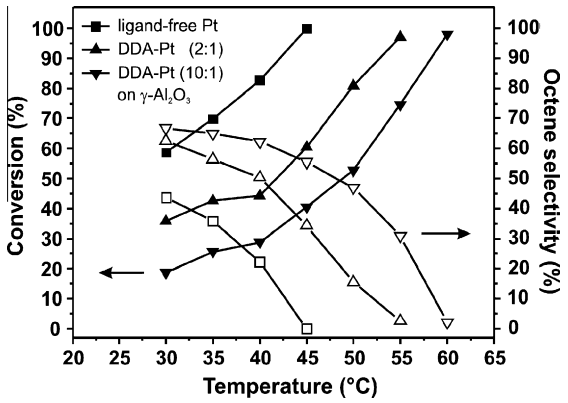

Fig. 2. Catalytic hydrogenation of 1,7-octadiene: activities and selectivities obtained for ligand-free and DDA-capped Pt nanoparticles supported on γ-Al_2O_3 (0.9 vol.% 1,7-octadiene, 7 vol.% H_2 in He, total gas flow: 50 mL/min). Full symbols depict octadiene conversion, open symbols selectivity to octene (mainly 1-octene, other octene isomers are not formed in significant amounts under the conditions applied).

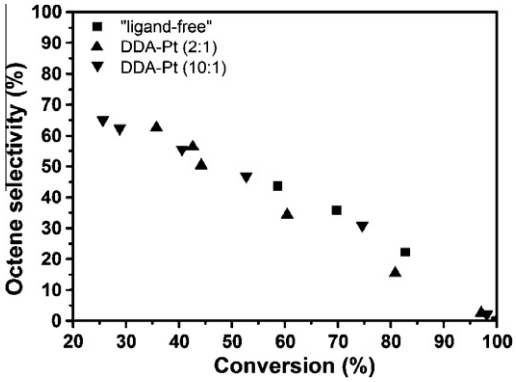

Fig. 3. Catalytic hydrogenation of 1,7-octadiene: octene selectivities of ligand-free and DDA-capped Pt nanoparticles supported on γ-Al_2O_3 plotted as a function of octadiene conversion (0.9 vol.% 1,7-octadiene, 7 vol.% H_2 in He, total gas flow: 50 mL/min). (Please note that under the conditions applied 1-octene was the only isomer of octene that was formed in significant amounts.)

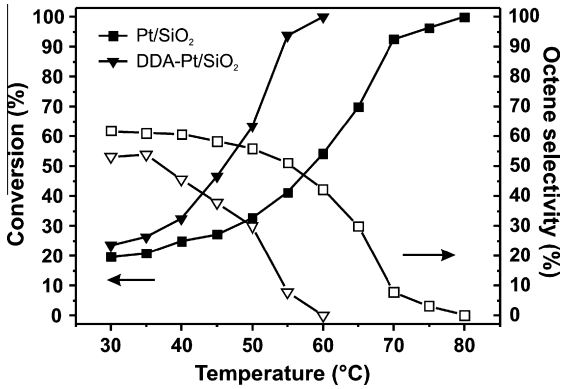

Fig. 4. Catalytic hydrogenation of 1,7-octadiene: activities and selectivities of ligand-free and DDA-capped Pt nanoparticles supported on SiO_2 (0.9 vol.% 1,7-octadiene, 7 vol.% H_2 in He, total gas flow: 50 mL/min). Full symbols depict octadiene conversion, open symbols selectivity to octene (mainly 1-octene, other octene isomers are not formed in significant amounts under the conditions applied).

the same light-off temperature for converting CO to CO_2, revealing that the type of support apparently does not play an important role for the performance of the ligand-free Pt catalysts in the case of CO oxidation.

Turning to the DDA-capped Pt nanoparticles, a different behavior is observed. While the γ-Al_2O_3-supported particles exhibit essentially the same light-off temperature as the unprotected particles, *distinct* differences in the catalytic activity are discernible for particles on other supports. The activities of the DDA-capped Pt catalysts decrease in the following order: γ-Al_2O_3 > MgO > SiO_2 (Fig. 5). This result is rather unexpected as the ligand shell should lead to the same catalytic activity in all cases as was observed for the hydrogenation experiments. To check whether the observed activity sequence is a general phenomenon, DDA–Pt particles on γ-Al_2O_3 and SiO_2 were also prepared by using a classical colloidal approach [2] and exemplarily investigated under the same reaction conditions. The results revealed an identical trend with respect to the activity: The light-off temperature for CO oxidation in the case of SiO_2-supported particles was 20–30 °C higher than that for γ-Al_2O_3-supported ones.

The stability of the ligand-free and DDA-capped Pt catalysts was investigated by using the catalysts in a second catalytic experiment. Changes in the activities of the ligand-free Pt/γ-Al_2O_3, Pt/MgO and Pt/SiO_2 catalysts between the 1st and 2nd runs of the reaction were negligible, suggesting that the systems are structurally stable under the reaction conditions, e.g., with respect to sintering. All ligand-capped catalysts, on the other hand, exhibit slightly increased activities in the second measurement. A comparison on the STEM images of the fresh catalysts (Fig. 1c and d) and the recycled ones (Fig. 1e and f) however reveals that no obvious changes in the size and shape of the Pt nanoparticles occurred during the reaction.

3.4. IR spectroscopic characterization

Turning to the ligand-free samples first, the top spectra in Fig. 6a and c and e depict CO adsorption spectra of Pt supported on MgO, γ-Al_2O_3 and SiO_2, respectively. Interestingly, significant differences between these three spectra are obvious: In the case of MgO (Fig. 6a), the main peak in the CO region at 2060 cm^{-1} can be assigned to CO adsorbed linearly on metallic Pt, while the smaller peak at 2082 cm^{-1} points to small amounts of partially oxidized Pt [42]. Although the main peak at 2060 cm^{-1} is present on the alumina-supported sample (Fig. 6c) too, the second blue-shifted peak is absent. However, an additional peak with low intensity at 2248 cm^{-1} is visible that can be assigned to a Pt^{2+} carbonyl species [43]. When using SiO_2 as a support (Fig. 6e), not only the CO atop band is blue-shifted by ~20 cm^{-1} when compared to the two other supports, but in addition, and more importantly, pronounced signals of CO adsorbed on oxidized Pt species [43] (2110, 2146 and 2182 cm^{-1}) appear in the IR spectrum.

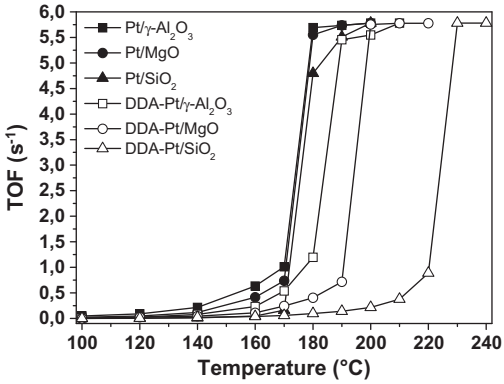

Fig. 5. Turnover frequencies (CO_2 molecules formed per s and per Pt atom) for CO oxidation over ligand-free and DDA-capped Pt nanoparticles deposited on different oxide supports. Reaction conditions: 3 vol.% of CO in synthetic air; total velocity of gas flow: 50 mL/min.

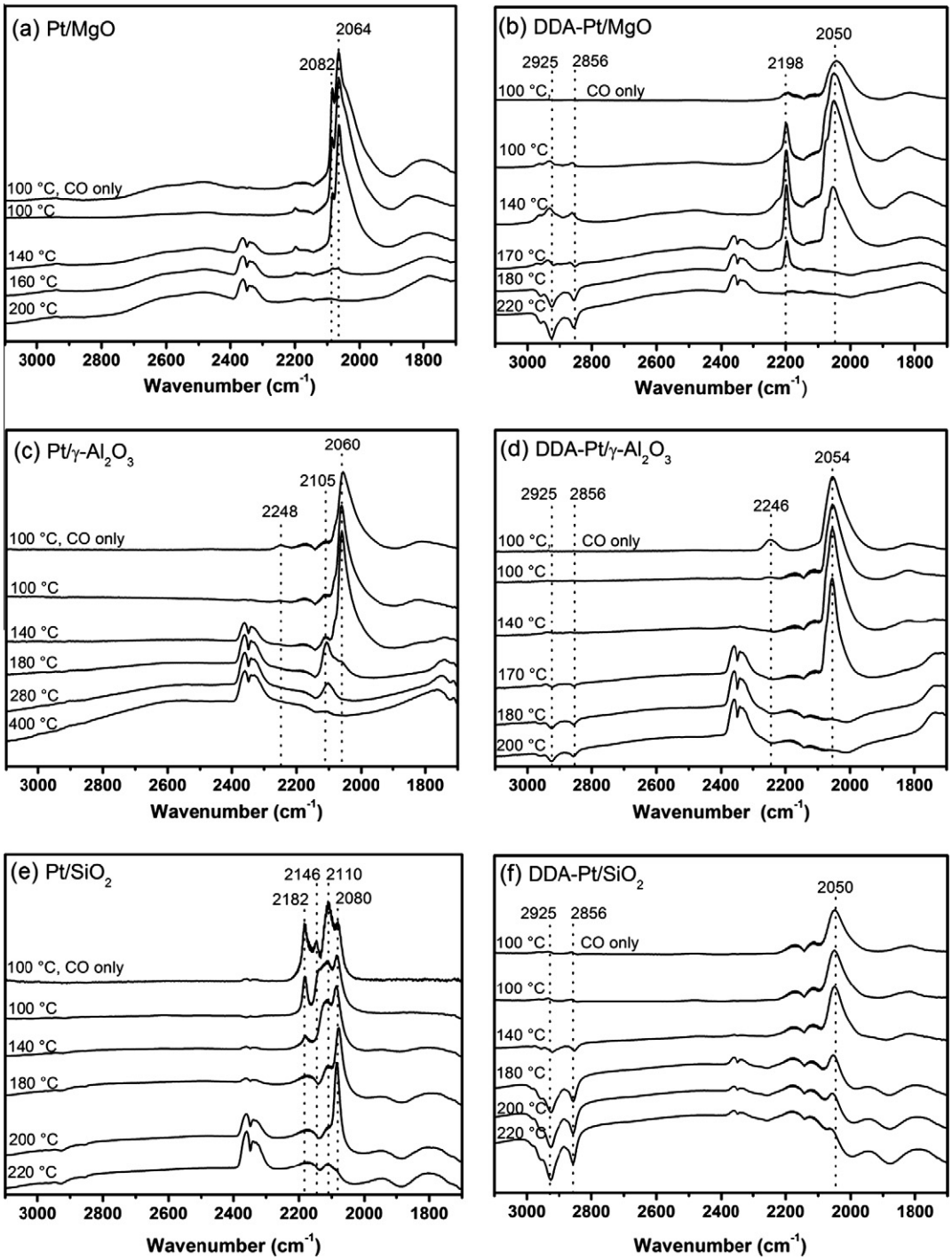

Fig. 6. In-situ IR spectra of CO oxidation over ligand-free and DDA-capped Pt catalysts: (a) Pt/MgO; (b) DDA–Pt/MgO; (c) Pt/γ-Al_2O_3; (d) DDA–Pt/γ-Al_2O_3; (e) Pt/SiO_2; (f) DDA–Pt/SiO_2. Reaction conditions: 1 vol.% of CO and 1 vol.% of O_2 in Ar; total velocity of gas flow: 200 mL/min.

The situation is different for the DDA-capped Pt samples: here, all peaks pointing to Pt surface oxidation are absent in the case of the silica-supported sample (Fig. 6f), meaning that all three supports show now a similar behavior with a peak of linear CO adsorption on metallic Pt sites at around 2050 cm^{-1}. The red-shift of this band with respect to the ligand-free catalysts can be interpreted as a sign for reduced dipole–dipole interactions between the adsorbed CO molecules, meaning that the ligand shell leads to more isolated adsorption sites. Just, the band at $\sim$2250 cm^{-1} on the Al_2O_3-sample due to Pt^{2+} carbonyls is comparable to that observed in the ligand-free case, suggesting that the formation of such carbonyl species is not influenced by the presence of the ligand shell.

In summary, CO adsorption experiments suggest that dependent on the support, surface oxidation of the Pt can take place to a different degree. In particular, silica leads to strong oxidation. If ligands are used, however, no such effect can be observed. These conclusions were essentially confirmed by additional XPS measurements carried out for the pristine samples. In the case of the ligand-free particles oxidized Pt was found, but only in limited amounts (<10 %) meaning that the surface is (partly) oxidized

during the deposition but *not the bulk*. Notably, also in the case of the ligand-capped particles, XPS indicated traces of oxidized Pt. This observation can be explained by corresponding species at the interface to the silica support, implying that – in contrast to the surface, where the ligands effectively prevent oxidation according to DRIFTS – they do not necessarily prevent the interaction at the bottom side of the particles.

In order to gain further insight into the fate of the various surface species under reaction conditions, also CO oxidation experiments were performed in the DRIFTS cell. As shown in Fig. 6a for the ligand-free Pt/MgO catalyst, an obvious CO_2 gas-phase absorption band (centered around 2340 cm^{-1}) occurs at 140 °C, suggesting that, at this temperature, the CO oxidation starts. The strong peak at 2060 cm^{-1} due to CO atop adsorption on Pt^0 as well as the shoulder at 2082 cm^{-1} assigned to CO adsorption on partially oxidized Pt disappear at temperatures higher than 160 °C, indicating that these CO species take place in the reaction.

Turning to the alumina-supported sample (Fig. 6c), the band at 2248 cm^{-1} observed in the CO adsorption experiments is not present at higher temperatures under oxidative conditions, suggesting decomposition of the carbonyl species under these circumstances. An additional small absorption band around 2105 cm^{-1} emerges at 180 °C after the onset of catalytic activity, i.e. the appearance of a CO_2 signal. This band can be related [43] to the adsorption of CO on Pt^+ originating from surface oxidation. It was reported that the Pt^+–CO complexes are very stable and their stability is a consequence of the synergistic effect of the σ bonds and the π backbonds, which is possible for Pt cations in low oxidation states. At higher temperatures, however, the band decreases again.

Finally, the spectra of the silica-supported sample (Fig. 6e) under CO oxidation conditions resemble the one for CO adsorption at 100 °C. At higher temperatures, however, the dominant peaks of CO adsorbed on oxidized Pt disappear even earlier than the band assigned to CO on metallic Pt (2080 cm^{-1}), showing that in contrast to Al_2O_3 no oxidized species with high thermal stability were created.

When comparing the DDA-capped particles (right-hand side of Fig. 6) to the ligand-free Pt particles (left-hand side of Fig. 6) on the same support, also under oxidative conditions all absorption bands which we could relate to surface oxidation of Pt are absent. The bands due to CO atop adsorption can virtually be found at the same position (~2050 cm^{-1}) in all three cases. This clearly points to a ligand-induced protection of the Pt cores against oxidation also under reaction conditions. A – at first sight unexpected – band occurs for the DDA-capped Pt on MgO. This band at 2198 cm^{-1}, however, is *not* related to Pt surface oxidation and will be discussed in Section 4.2 in detail.

A second region in the IR spectra showing temperature-induced changes is found between 2850 and 3000 cm^{-1}, where the C–H stretching vibrations appear. Here, small negative bands occur at temperatures higher than 170–180 °C, pointing to a certain loss of the ligands. This is consistent with TGA measurements on the DDA–Pt sample (Fig. 7) showing some weight loss in the temperature range below 200 °C. This loss, however, is small and concerns only ~20% (corresponding to 5 wt.%) of the ligands, suggesting that most of the ligands are still present.

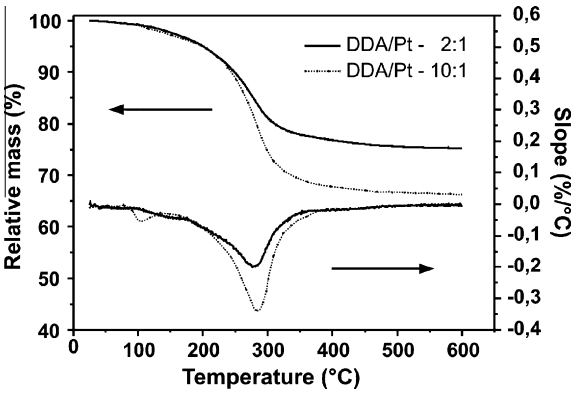

Fig. 7. TGA data: relative mass loss and first derivative of the curves for DDA-capped Pt nanoparticles prepared with different molar ratios of ligands to Pt (2:1 and 10:1, respectively).

4. Discussion

4.1. Support dependent differences in the catalytic activity of the ligand-free Pt nanoparticles

In the case of the ligand-free Pt nanoparticles, our approach using the same Pt nanoparticles and depositing them in the same way on different supports enables us to compare the specific metal–support interactions in detail. The differences in the IR spectra clearly indicate a support dependent oxidation of Pt surface atoms with the degree of oxidation decreasing in the following order: SiO_2 > Al_2O_3 > MgO. This trend can be correlated with the different Brønsted acidity of the supports since it is known [44] that Brønsted acidic supports are able to oxidize Pt by reduction of hydroxyl groups. In agreement with the Brønsted acidity of silica [45], the highest degree of oxidation occurs on this support. In contrast, hardly any oxidation was observed on the basic magnesia showing no Brønsted acidity at all. For alumina the presence of Brønsted acidic sites was reported when this generally Lewis acidic oxide is exposed to moisture [44]. Accordingly, its ability to oxidize Pt can be expected to lie between silica and magnesia, as indeed observed.

It is worthwhile to recall that, although these distinct differences regarding the various supports can be detected in the DRIFT spectra, the catalytic behavior with respect to CO oxidation in the reactor was comparable. Apparently, the surface oxides formed as a consequence of the metal–support interaction do not decrease the catalytic activity significantly, probably because they decompose or get reduced by CO in the temperature region where catalytic activity sets in. (Note that Pt oxide species formed *during* reaction at higher temperatures – as observed in the form of Pt^+–CO on alumina – do not lead to an observable effect since the activity is very high here and full conversion is reached.)

As far as the hydrogenation activity of the ligand-free Pt nanoparticles is concerned, the situation is different. Here, only the particles on γ-Al_2O_3 and MgO showed comparable results, whereas significantly lower activity is observed for SiO_2 as a support. Since it is known [46] that oxidized Pt species are in general significantly less active for hydrogenation reactions, it seems that in the case of the hydrogenation reaction the surface oxidation being most pronounced on SiO_2 leads to a noticeable reduction of the catalytic activity (shift of the conversion curve to about 30 °C higher temperatures compared to the Al_2O_3 and MgO samples).

To further support this interpretation, additional reduction experiments were performed with the ligand-free Pt/SiO_2 sample. Fig. 8 shows that 2 h in a H_2 flow at 200 °C and 300 °C led to a shift of the conversion curves by 5 °C and 10 °C to lower temperatures, respectively. This result supports the fact that the oxidized species are causing the lower activity for octadiene hydrogenation. Nevertheless, it is obvious that even a subsequent reduction cannot shift the activity to a range found for the MgO or Al_2O_3-supported sample.

4.2. Ligand-capped Pt nanoparticles: Fate of the ligands

While different activities for CO oxidation on the ligand-free particles might have been expected because of a more pronounced

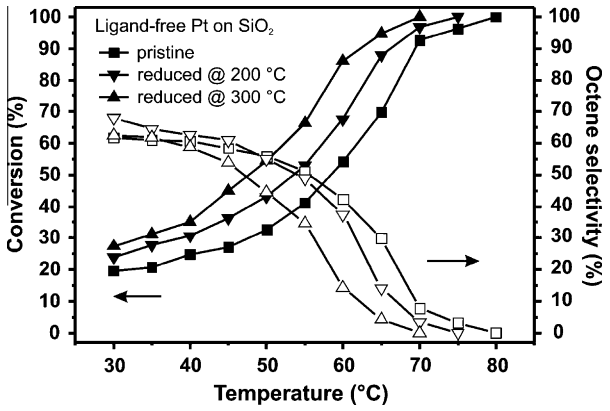

Fig. 8. Catalytic hydrogenation of 1,7-octadiene: activities and selectivities of ligand-free Pt supported on SiO_2 (0.9 vol.% 1,7-octadiene, 7 vol.% H_2 in He, total gas flow: 50 mL/min); pristine and reduced at 200 or 300 °C (2 h, 50 mL H_2/min) respectively. Full symbols denote octadiene conversion, open symbols selectivity to octene (mainly 1-octene, other octene isomers are not formed in significant amounts under the conditions applied).

surface oxidation of Pt on some supports, the *observed* differences for the ligand-capped particles are surprising at first sight. Having a closer look on the data, however, reveals an interesting detail in the case of the MgO-supported DDA–Pt particles. Here, the aforementioned IR absorption band at 2198 cm^{-1} appears in the spectrum whose intensity first increases with reaction temperature and then disappears at temperatures above 200 °C (Fig. 6b). Based on former work [31], the position of this band is consistent with a nitrile species which originates from a reaction of the amine ligands with the MgO support. In other words, this band provides clear evidence that partial spillover of the DDA ligands to the support can take place.

The fact that a similar band is not detected for amine-capped particles on the other supports does not mean that ligand spillover does not occur here since nitrile formation can only take place on magnesia and not on the other supports used in this study. In a previous study [31], spillover of ligands was also reported for alumina supports. The origin of such a spillover could be acid–base interactions between ligands and the surface of the supports based on their acidity. Taking the different surface acidities of the support materials used in this study into account, different degrees of spillover leading to different ligand coverages on the surface of the particles provide a comprehensible explanation for the trends. While on SiO_2 substantial spillover of the basic amine ligands is not expected because of the missing Lewis acidity, the high Lewis acidity of γ-Al_2O_3 enables a larger degree of spillover. A high degree of spillover of course means a larger number of free Pt surface sites for CO oxidation and consequently a higher catalytic activity.

This interpretation was confirmed by an additional CO oxidation experiment carried out with DDA–Pt nanoparticles deposited on a γ-Al_2O_3 support *presaturated* with DDA. It was found that the results were similar to DDA–Pt nanoparticles deposited on pristine SiO_2. So, if the ligand spillover is inhibited on the catalyst surface, the catalytic properties of the ligand-capped nanoparticles become independent of the support materials.

However, while the acid/base properties of the supports can explain the behavior in case of the SiO_2-and γ-Al_2O_3-supported particles, MgO does not fit into the trend of the surface acidity, as it shows an even lower Lewis acidity than SiO_2. Here, however, the formation of the nitrile due to the chemical interaction between the amine ligands and the MgO support, as discussed above, most probably drives the ligand spillover.

Besides spillover, of course, also decomposition and/or desorption of the ligands cannot be disregarded at the high temperatures (~200 °C) under CO oxidation conditions, which was confirmed by the TGA data shown in Fig. 7. However, neither blocking of the Pt surface by decomposition products was observed nor a full removal of the ligands can be expected under such conditions. Apparently ligand spillover has a much stronger influence on catalytic CO oxidation over ligand-capped Pt nanoparticles than other possible ways of ligand removal.

In contrary, hydrogenation reactions provide insight into the influence of ligands at low temperatures ($T < 100$ °C) where ligand decomposition/desorption and possibly spillover can be disregarded. As can be seen from Fig. 2, in the case of the alumina-supported samples obviously the catalytic activity for 1,7-octadiene hydrogenation does only depend on the amount of ligands on the Pt surface, in other words on the number of free Pt sites: the conversion curve for the highest DDA-coverage (ratio DDA/Pt: 10/1) is shifted to about 15 °C higher temperatures compared to the ligand-free particles. Nevertheless, octadiene can penetrate the ligand shell to an appreciable extent also for dense ligand shells. To this end, spillover of ligands onto the support indeed seems not to play a significant role at such low temperatures under hydrogenation conditions.

4.3. Influence of the ligands on the surface and catalytic properties of the Pt nanoparticles

In spite of a partial loss of ligands due to spillover and decomposition/desorption at higher temperatures, they effectively protect the Pt nanoparticles against surface oxidation, as clearly revealed by the DRIFTS data. Since the oxidation is obviously driven by metal–support interactions, probably occurring already during deposition of the particles, it is likely that the protecting effect of the ligands is based on a decoupling of the particles from the support.

As discussed in Section 4.1, in the case of *CO oxidation* the protecting effect of the ligand shell against surface oxidation of the Pt nanoparticles has no detectable influence on the catalytic behavior. Here, rather the ligands decrease the activity due to blocking of surface sites. Turning to octadiene hydrogenation, however, the situation is distinctly different. While in the case of γ-Al_2O_3 and MgO the DDA-capped samples exhibit a lower activity compared to the ligand-free samples (10 °C upshifted) due to the blocking of some active (metallic) surface sites, the conversion curve of the DDA-capped Pt/SiO_2 is 20 °C *downshifted* compared to naked Pt/SiO_2. In agreement with the DRIFTS data, this observation suggests that the protection against oxidized Pt species which strongly decrease catalytic activity by far outweighs the blocking effect, resulting in a higher activity of the ligand-capped Pt/SiO_2 compared to the ligand-free sample.

However, the activity of the ligand-free sample reduced at 300 °C is still significantly lower than the DDA-capped Pt/SiO_2 (another 10 °C shift). Thus – also having aspects like sintering in mind – a sample with comparable activity cannot be easily obtained by reduction of a ligand-free Pt/SiO_2 sample, emphasizing the beneficial effect of a protecting ligand shell.

5. Conclusions

It could be shown that the ligand shell of Pt nanoparticles leads to a certain blocking of active surface sites but also has a protecting function with respect to support induced surface oxidation by suppressing metal–support interactions during the deposition.

Although infrared measurements prove that in the case of ligand-free nanoparticles on the different supports varying amounts of oxidized Pt species are present, the CO oxidation activity does not notably decrease because they decompose or

get reduced again in the higher temperature region of the reaction onset.

In contrast, all ligand-capped samples were less active for CO oxidation due to partial blocking of surface sites. However, differences were detected for different support materials dependent on their acid/base and catalytic properties, which determine the degree of ligand spillover decreasing from γ-Al_2O_3 > MgO > SiO_2. The same trends were also observed for nanoparticles prepared by a classical colloidal synthesis method and are thus not limited to the ethylene glycol method.

At low temperatures (T < 100 °C), however, the differences between particles with and without ligands were more pronounced since the ligand shell is intact under these conditions and spillover probably does not yet play a role. Interestingly, whereas for the γ-Al_2O_3-and MgO-supported samples the catalytic activity for octadiene hydrogenation decreased with increasing amount of ligands due to the blocking effect, a clearly beneficial influence of the ligand shell could be found for the silica-supported sample. Here, the significantly higher activity of the ligand-capped sample compared to ligand-free Pt was attributed to a very efficient protection against surface oxidation by the ligands.

By virtue of this effect, supported ligand-capped metal particles as obtained by many colloidal synthesis routes can sometimes result in catalysts, which are much more active as particles without a ligand shell.

Our work shows that studies on ligand-capped nanoparticles aiming e.g. at an elucidation of the effect of the organic ligands on activity and selectivity in catalytic applications need to consider different aspects such as reaction conditions, acid/base properties of the support and spillover of ligands. Furthermore, ligand capping may open up new perspectives for the development of catalysts in cases where a partial oxidation of the metal nanoparticles during the catalytic reaction is not desirable.

Acknowledgments

Financial support of the DFG is gratefully acknowledged. Furthermore, we thank Prof. Dr. M. Wickleder (University of Oldenburg) for the TGA measurements. Xiaodong Wang is grateful for a fellowship of the Hanse-Wissenschaftskolleg (Hanse Institute for Advanced Study).

References

[1] D.V. Leff, L. Brandt, J.R. Heath, Langmuir 12 (1996) 4723.
[2] N.R. Jana, X. Peng, J. Am. Chem. Soc. 125 (2003) 14280.
[3] F. Pinna, Catal. Today 41 (1998) 129.
[4] F.C. Patcas, G.I. Garrido, B. Kraushaar-Czarnetzki, Chem. Eng. Sci. 62 (2007) 3984.
[5] G. Schmid, Chem. Rev. 92 (1992) 1709.
[6] S. Sun, C.B. Murray, D. Weller, L. Folks, A. Moser, Science 287 (2000) 1989.
[7] T. Hyeon, Chem. Commun. (2003) 927.
[8] S. Chen, R.S. Ingram, M.J. Hostetler, J.J. Pietron, R.W. Murray, T.G. Schaaff, J.T. Khoury, M.M. Alvarez, R.L. Whetten, Science 280 (1998) 2098.
[9] S.-Y. Zhao, S.-H. Chen, S.-Y. Wang, D.-G. Li, H.-Y. Ma, Langmuir 18 (2002) 3315.
[10] E.V. Shevchenko, D.V. Talapin, A.L. Rogach, A. Kornowski, M. Haase, H. Weller, J. Am. Chem. Soc. 124 (2002) 11480.
[11] E.V. Shevchenko, D.V. Talapin, H. Schnablegger, A. Kornowski, O. Festin, P. Svedlindh, M. Haase, H. Weller, J. Am. Chem. Soc. 125 (2003) 9090.
[12] I. Quiros, M. Yamada, K. Kubo, J. Mizutani, M. Kurihara, H. Nishihara, Langmuir 18 (2002) 1413.
[13] J. Yang, T.C. Deivaraj, H.-P. Too, J.Y. Lee, J. Phys. Chem. B 108 (2004) 2181.
[14] S.-W. Kim, J. Park, Y. Jang, Y. Chung, S. Hwang, T. Hyeon, Y.W. Kim, Nano Lett. 3 (2003) 1289.
[15] Z.L. Wang, Z. Dai, S. Sun, Adv. Mater. 12 (2000) 1944.
[16] V.F. Puntes, K.M. Krishnan, P. Alivisatos, Appl. Phys. Lett. 78 (2001) 2187.
[17] E. Shevchenko, D. Talapin, A. Kornowski, F. Wiekhorst, J. Kötzler, M. Haase, A. Rogach, H. Weller, Adv. Mater. 14 (2002) 287.
[18] J. Turkevich, G. Kim, Science 169 (1970) 873.
[19] M. Comotti, W.-C. Li, B. Spliethoff, F. Schüth, J. Am. Chem. Soc. 128 (2006) 917.
[20] H. Lang, R.A. May, B.L. Iversen, B.D. Chandler, J. Am. Chem. Soc. 125 (2003) 14832.
[21] T.O. Hutchinson, Y.P. Liu, C. Kiely, C.J. Kiely, M. Brust, Adv. Mater. 13 (2001) 1800.
[22] H. Bönnemann, G.A. Braun, Angew. Chem. Int. Ed. 35 (1996) 1992.
[23] T. Mallat, E. Orglmeister, A. Baiker, Chem. Rev. 107 (2007) 4863.
[24] E. Schmidt, W. Kleist, F. Krumeich, T. Mallat, A. Baiker, Chem. Eur. J. 16 (2010) 2181.
[25] J. Park, C. Aliaga, J. Renzas, H. Lee, G.A. Somorjai, Catal. Lett. 129 (2009) 1.
[26] J.N. Kuhn, C.-K. Tsung, W. Huang, G.A. Somorjai, J. Catal. 265 (2009) 209.
[27] Y. Tai, W. Yamaguchi, M. Okada, F. Ohashi, K-i. Shimizu, A. Satsuma, K. Tajiri, H. Kageyama, J. Catal. 270 (2010) 234.
[28] H. Borchert, D. Fenske, J. Kolny-Olesiak, J. Parisi, K. Al-Shamery, M. Bäumer, Angew. Chem. Int. Ed. 46 (2007) 2923.
[29] K.M. Bratlie, H. Lee, K. Komvopoulos, P. Yang, G.A. Somorjai, Nano Lett. 7 (2007) 3097.
[30] K.M. Bratlie, K. Komvopoulos, G.A. Somorjai, J. Phys. Chem. C 112 (2008) 11865.
[31] B. Jürgens, H. Borchert, K. Ahrenstorf, P. Sonström, A. Pretorius, M. Schowalter, K. Gries, V. Zielasek, A. Rosenauer, H. Weller, M. Bäumer, Angew. Chem. Int. Ed. 47 (2008) 8946.
[32] Y. Wang, J. Ren, K. Deng, L. Gui, Y. Tang, Chem. Mater. 12 (2000) 1622.
[33] Y. Wang, J. Zhang, X. Wang, J. Ren, B. Zuo, Y. Tang, Top. Catal. 35 (2005) 35.
[34] Y. Wang, H. Yang, Chem. Commun. (2006) 2545.
[35] C. Morterra, G. Magnacca, Catal. Today 27 (1996) 497.
[36] B.C. Beard, Z.C. Zhang, Catal. Lett. 82 (2002) 1.
[37] B.A. Morrow, I.A. Cody, J. Phys. Chem. 80 (1976) 1995.
[38] C. Scholfield, R. Butterfield, H. Dutton, J. Am. Oil Chem. Soc. 49 (1972) 586.
[39] R.S. Miner, K.G. Ione, S. Namba, J. Turkevich, J. Phys. Chem. 82 (1978) 214.
[40] X. Fu, Y. Wang, N. Wu, L. Gui, Y. Tang, J. Colloid Interface Sci. 243 (2001) 326.
[41] Z. Dobrovolná, P. Kacer, L. Cervený, J. Mol. Catal. A 130 (1998) 279.
[42] P.J. Lévy, V. Pitchon, V. Perrichon, M. Primet, M. Chevrier, C. Gauthier, J. Catal. 178 (1998) 363.
[43] K.I. Hadjiivanov, G.N. Vayssilov, Adv. Catal. 47 (2002) 307.
[44] Z.C. Zhang, B.C. Beard, Appl. Catal. A 188 (1999) 229.
[45] S. Eulig, M. O'Connor, H.P. Boehm, Z. Anorg. Allg. Chem. 464 (1980) 80.
[46] C.-S. Chen, H.-W. Chen, W.-H. Cheng, Appl. Catal. A 248 (2003) 117.